International Journal of Pharmaceutics 647 (2023) 123520

Contents lists available at ScienceDirect

International Journal of Pharmaceutics

journal homepage: www.elsevier.com/locate/ijpharm

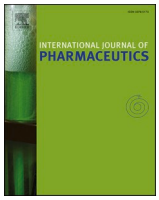

Elucidating the hydrotropism behaviour of aqueous caffeine and sodium benzoate solution through NMR and neutron total scattering analysis

Yichun Shen [a], Yitian Xiao [a], Robert M. Edkins [b], Tristan G.A. Youngs [c], Terri-Louise Hughes [c], James Tellam [d], Katharina Edkins [a,*]

[a] School of Health Sciences, University of Manchester, Stopford Building, Oxford Road, Manchester M13 9PT, UK
[b] Department of Pure and Applied Chemistry, University of Strathclyde, Thomas Graham Building, 295, Cathedral Street, Glasgow, G1 1XL, UK
[c] ISIS Pulsed Neutron and Muon Source, STFC Rutherford Appleton Laboratory, Harwell Oxford, Didcot, OX11 0QX, UK
[d] ISIS Deuteration Facility, STFC Rutherford Appleton Laboratory, Harwell Oxford, Didcot, OX11 0QX, UK

ARTICLE INFO

Keywords:
Solubility
Solution stucture
Simulation
Pharmaceutical

ABSTRACT

Hydrotropism is a convenient way to increase the solubility of drugs by up to several orders of magnitude, and even though it has been researched for decades with both experimental and simulation methods, its mechanism is still unknown. Here, we use caffeine/sodium benzoate (CAF-SB) as model system to explore the behaviour of caffeine solubility enhancement in water through NMR spectroscopy and neutron total scattering. ^{1}H NMR shows strong interaction between caffeine and sodium benzoate in water. Neutron total scattering combined with empirical potential structure refinement, a systematic method to study the solution structure, reveals π-stacking between caffeine and the benzoate anion as well as Coulombic interactions with the sodium cation. The strongest hydrogen bond interaction in the system is between benzoate and water, which help dissolve CAF-SB complex and increase the solubility of CAF in water. Besides, the stronger interaction between CAF and water and the distortion of water structure are further mechanisms of the CAF solubility enhancement. It is likely that the variety of mechanisms for hydrotropism shown in this system can be found for other hydrotropes, and NMR spectroscopy and neutron total scattering can be used as complementary techniques to generate a holistic picture of hydrotropic solutions.

1. Introduction

In pharmaceutical industry, less than one percent of active pharmaceutical ingredients (API) can become commercial medicines because of their poor biopharmaceutical properties such as solubility rather than their toxicity (Aakeroy et al., 2009). It has been reported that APIs with insufficient solubility show poor *in vitro* (Cheng and Coon, 1990) and *in vivo* (Telange et al., 2017) performance, problematic formulation development and bad bioavailability (Savjani et al., 2012). Therefore, a number of techniques have been developed to improve the poor solubility of drugs, mainly based on particle size reduction by using mechanical force (Loh et al., 2015), nanotechnology (Alshora et al., 2016) or crystallisation from supercritical fluid (Misra and Pathak, 2020). However, the high surface charge caused by the small particle size results in powder agglomeration and cohesiveness, which poses a further challenging problem in the manufacture of medicines (Vemula and Srikanth Lingala, 2010). Besides, crystal engineering methods have been researched for decades including transferring original crystal forms into the amorphous phase (Mishra et al., 2015) or other metastable polymorphs (Martinez et al., 2022). The higher energy of these materials lead to significant instability and the tendency of re-crystallization into a more stable crystal form (Yamamoto et al., 2016). In addition to single-component crystal structures, multi-component crystal forms have been investigated for their ability to increase the solubility of APIs, e.g. the formation of salts (Serajuddin, 2007), hydrates (Jangid et al., 2019) and co-crystals (Thakuria et al., 2013). Avoiding the necessity to change the drug's crystal form, the addition of a second solute molecule can lead to hydrotropism, which can increase the solubility of APIs up to several orders of magnitude (Könczöl and Dargó, 2018; Subbarao et al., 2012).

Hydrotropes have amphiphilic structures and can hugely increase the solubility of sparingly soluble organic molecules in water (Kunz et al., 2016; Lee et al., 2003). The most common structure of hydrotropes is a hydrocarbon ring combined with an ionic moiety (Hodgdon and Kaler, 2007) but the class of hydrotropic molecules shows a large

* Corresponding author.
E-mail address: katharina.edkins@manchester.ac.uk (K. Edkins).

https://doi.org/10.1016/j.ijpharm.2023.123520
Received 1 June 2023; Received in revised form 13 October 2023; Accepted 16 October 2023
Available online 17 October 2023

variety of other structures. Although hydrotropism is widely used in the pharmaceutical industry, its molecular principles are still not clear (Dhapte and Mehta, 2015). Different hypotheses have been proposed: The self-aggregation of hydrotropes is regarded as the major driving force of the solubility enhancement phenomenon in many studies (Balasubramanian et al., 1989; Cui, 2010; Cui et al., 2010); while the interaction between hydrotropes and solute plays an important role to increase the solubility in other cases (Hussain et al., 1993; Sanghvi et al., 2007). The disruption and restoration of water hydrogen bonds are not negligible (Cui, 2010; Dhapte and Mehta, 2015). It is likely that the difficulty in explaining the mechanism of hydrotropism lies in different dominant mechanisms in hydrotropes of similar structures (Lee et al., 2003). It is also unknown what determines the minimum hydrotrope concentration, a threshold concentration for solubilization, and Shimizu *et al.* (Shimizu and Matubayasi, 2014) propose that the key to understand the hydrotrope concentration is the interaction between hydrotrope with water around the solute molecules.

Various techniques have been used to explore the mechanism of hydrotropism for small molecule hydrotropes. The majority of studies have used the common techniques of UV–Visible absorption spectroscopy (Coffman and Kildsig, 1996; Kumar et al., 2021), infrared spectroscopy (Lee et al., 2003) and nuclear magnetic resonance (NMR) spectroscopy (Rasool et al., 1991), where peak shifts of the pure drug have been seen after the addition of hydrotropes. Molecular dynamics (MD) simulations have also been applied (Cui, 2010; Cui et al., 2010) and both experimental and simulation methods have proposed several possible mechanisms.

However, while the spectroscopic observation of peak shift alone can be used to confirm the interaction and calculate the Gibbs free energy of interaction, it is challenging to determine the solution structure. Many simulation studies lack crucial experimental data, making it difficult to show the real structure and interactions among the solute, hydrotrope, and water in a solution. In this study, we use neutron total scattering to research the structure of small molecule hydrotropes in solution on a molecular level and elucidate the mechanism of hydrotropism.

Sodium benzoate (SB), containing benzoate (BEN) anion and sodium cation (Na^+), is a well-known hydrotropic agent. (Hodgdon and Kaler, 2007; Kumar et al., 2021; Tripathi et al., 2022) SB is a monomeric hydrotrope (Hopkins Hatzopoulos et al., 2011) without surfactant characteristics, which means it is different from any of the micelle hydrotropes and will not cause the formation of a microemulsion (Han et al., 2022; Shimizu and Matubayasi, 2017; Zemb et al., 2016). Researchers found by using infrared spectroscopy that SB interacts with promethazine hydrochloride observing a shift in the C-N and C–H stretch and C–H bend vibrations, while UV–Visible absorption spectroscopy showed a blue shift of the drug absorption in the mixed system (Kumar et al., 2021). The interaction between imipramine hydrochloride and SB has been found through the reduced fluorescence intensity of the drug with different concentration of SB (Rub, 2020). However, the structural details of these interactions and aggregation in solution are still unknown. Caffeine (CAF) is a cheap, easily available and widely used psychoactive drug, with low aqueous solubility of 0.1 M at room temperature (Tavagnacco et al., 2015). This solubility is particularly challenging since caffeine has been suggested and used as injection in the treatment of respiratory depression associated with overdose of CNS depressant drugs, e.g. narcotics or alcohol, or may be administered to neonates to treat apnoea (Gorodischer and Karplus, 1982). Besides, it has been reported that CAF-SB has a sunscreen effect (Lu et al., 2007) and can be applied to relieve postural puncture headaches (Yucel et al., 1999). Therefore, we concentrate in this work on investigating the mechanism of hydrotropism by using NMR spectroscopy and neutron total scattering in the model system CAF-SB.

2. Materials and methods

2.1. Materials

CAF, SB and D_2O were purchased from Sigma-Aldrich. The purity of the deuterated solvent was $\geq$ 99.8% and all chemicals were used without further purification. Ultrapure water was obtained by Synergy® UV purification system.

2.2. Synthesis of deuterated SB

Deuterated SB (SB-D5) was synthesized by the ISIS Deuteration facility lab, as follows:

Sodium benzoate (20.0 g, 139 mmol, 1 equiv.) and Pt/C (1.4 g, 6.94 mmol, 0.05 equiv.) were combined in D_2O (320 mL) and heated at 180 °C in a Parr reactor for 3 days. The reactor was cooled and the D_2O was removed by freeze-drying. The residue was resuspended in D_2O (320 mL) and heated at 180 °C in a Parr reactor for a further 3 days. The reactor was then cooled, and the solution was filtered, adjusted to pH = 1 with concentrated HCl and extracted with ethyl acetate. The organic phase was dried over $MgSO_4$, filtered, and concentrated *in vacuo* to afford benzoic acid-d5. Benzoic acid-d5 was suspended in D_2O and treated with 1 M NaOH solution to pH = 7. The solution was centrifuged to remove any residual carbon and then freeze dried to afford sodium benzoate-d5 as a white solid (17 g, 82 %).

2.3. Solubility measurement

To measure the solubility of CAF and SB, excess CAF or SB was added into water to make a slurry. The slurry was stirred at room temperature in a sealed vial using a magnetic stirrer bar for 24 h. The solution was transferred into five pre-weighted vials using a syringe with a 0.22 μm PTFE filter. The mass of solution was recorded, and the vials were placed in the vacuum oven until the water evaporated. The mass of dried solute was then recorded.

To explore the minimum hydrotrope concentration (MHC), the threshold concentration of hydrotropes at which the solubility of the solute suddenly increases (Shimizu and Matubayasi, 2017), solutions with various concentration of SB were prepared. Excess CAF was added into each solution of SB and the solubility of CAF was measured according to the procedure above.

2.4. NMR titration

^{1}H NMR spectra were obtained on a Bruker Avance-III 300 spectrometer (Karlsruhe, Germany). The chemical shifts were assigned using dichloromethane (DCM, chemical shift: δ = 5.33 ppm) in capillary as standard. The data from the spectra were analysed using MestRe nova (Mnova) software (Mestrelab Research, A Coruña, Spain). The measured range of chemical shifts is from −4 to +16 ppm. A change in chemical shift ($\Delta\delta$) in all ^{1}H NMR experiments is regarded as significant if the peak shift value is larger than the instrument resolution of ± 0.002 ppm. For the sample preparation of the titration experiment, the host (CAF) stock solution without any guest (SB) was prepared at a concentration of 0.01 M. To make the guest stock solution with the largest guest molar ratio of 150:1, weighed guest solid was dissolved into the host stock solution to ensure the host concentration did not change during the experiment. The rest of the molar ratios were obtained by mixing different amounts of host and guest stock solution. The apparent binding constant (K) was computed using BindFit (Thordarson, 2011) and the apparent binding model was chosen according to the lowest error and chemical logic (Brocos et al., 2010; Guerrero-Martínez et al., 2006; Shen et al., 2023). The apparent Gibbs free binding energy (ΔG_{bind}) can be calculated by the equation (1):

$$\Delta G_{bind} = -RTlnK \quad (1)$$

in which R is the universal gas constant (8.314 J K^{-1} mol^{-1}), T is the absolute temperature and K is the apparent binding constant.

2.5. Neutron experiment

Neutron total scattering data were collected using the Near and InterMediate Range Order Diffractometer (NIMROD) instrument at the ISIS Neutron and Muon source (Harwell, UK). The instrument has 2268 detectors covering the wide angle range of $2\theta = 0.5 - 40^{\circ}$, which provides appropriate data collection from hydrogenous samples. The simultaneous momentum transfer (Q) range is from 0.02 to 50 $Å^{-1}$, calculated from $Q = 4\pi/(\lambda \sin\theta)$ with the neutron wavelengths $\lambda = 0.05 - 4.95$ A, allowing measurements for both atomistic and mesoscale structures.

Seven isotopic substituted liquid samples of 2.2 M CAF and 3.9 M SB in water solution were prepared and transferred into 36 × 36 × 1 mm^3 internal volume quartz cells, which were loaded onto the sample changer on NIMROD. For solvent–solvent correlations, CAF and SB-D_5 in D_2O, CAF and SB-D_5 in 1:1 mixture of H_2O:D_2O, and CAF and SB-D_5 in H_2O were used; for solute–solute correlations, data on CAF and 1:1 mixture of SB:SB-D_5 in D_2O, and CAF and SB in D_2O were collected; for solvent–solute correlations, CAF and 1:1 mixture of SB:SB-D_5 in 1:1 mixture of H_2O:D_2O, and CAF and SB in H_2O were investigated. The isotopic substitution was used to generate sufficient observations to generate a stable and precise simulation box and it was assumed that the solution structure does not change due to the isotope effect. All sample preparations and measurements were conducted at 25 °C and the liquid samples remained stable showing no signs of crystallization during the entire process. The samples were measured in 1-hour scans summed up to give at least 4 h of data acquisition per sample for appropriate signal-to-noise ratio and appropriate data statistics. The individual scans were checked to ensure sample stability and no crystallisation occurred during the experiment.

The program GudrunN was used for reduction and normalization of the measured data sets. It merges the data to an absolute Q-scale by normalizing to a 3 mm VNb plate calibration standard and subtracts the instrument and sample backgrounds from the experimental data. It also applies corrections for absorption and multiple scattering, and inelasticity effects due to the presence of light elements such as hydrogen (^1H), after which the total interference differential cross section, $F(Q)$, is obtained.

2.6. Dissolve simulation

The program Dissolve (Youngs, 2019) is used to simulate the three-dimensional atomic structure of the amorphous sample based on the neutron total scattering data. Dissolve builds on methodology established in the Empirical Potential Structure Refinement (EPSR) code (Soper, 1996), and provides the capability to simulate much larger and more complex systems with more flexibility than EPSR. The structure of CAF, BEN, water molecules and Na cation are created in Dissolve. For 2.2 M CAF with 3.9 M SB in water solution, the cubic box with the side length of 50.6341 Å was built containing 100 CAF, 186 BEN, 2631 water molecules and 186 Na^+. The density of the protonated solution was measured with an Anton Paar DMA 4100 M density meter at 1.1976 g/cm^3 with the corresponding atomic density of 0.100665 atoms $Å^{-3}$.

The standard OPLS-AA forcefield is applied to the molecules as their starting reference potentials, which provides information on their bonds, angles, and torsion angles as well as Lennard-Jones potentials. The electrostatic potential (ESP) atomic charges of the molecules are calculated using DFT on Gaussian 16 (Revision C). The molecular structures were optimised using [B3LYP/6-311G(d.p)] for C, H, N and O with a GD3BJ dispersion correction. Solvent (water) was included using the conductor-like polarizable continuum model (CPCM). ESP charges were calculated using the Merz–Kollmann model. The potential parameters are shown in ESI Table S1 according to the atom number labelled in Fig. 1. Other conditions, such as the atomic density number and temperature are applied to ensure the accuracy of the cubic simulation box. An iterative process involving the experimental data is used to form and apply an empirical potential to the simulation's pair potentials, in order to drive the simulation towards best agreement with the experimental data (for full details see (Youngs, 2019)).

The representations of the molecules in the simulation box were obtained using the Aten software (Youngs, 2010).

3. Results and discussion

3.1. Solubility test

The aqueous solubility of pure CAF and SB at room temperature is 0.10 M and 3.96 M, respectively. The trend of the CAF solubility increase is linear when SB concentration is lower than 1 M (ESI Figure S1), which means there is no point at which the solubility of CAF increases abruptly which would signify the minimum hydrotrope concentration. At higher concentrations of SB, the hydrotropic effect weakens as shown by a changed gradient. The solubility of CAF is increased by a factor of 3 in 0.35 M SB compared to pure water and up to as much as 22 times at a SB concentration of 3.96 M (ESI Table S2). Park *et al.* applied niacinamide and betaine as hydrotropic agents to enhance CAF solubility by around 3 and 1.2 times, respectively with the hydrotrope concentration of 0.4 M at room temperature (Park et al., 2022). Compared with the enhanced concentration of CAF in our study, it is obvious that SB is a good hydrotropic agent to enhance the poor solubility of CAF at room temperature even though the MHC does not exist.

3.2. NMR titration

To investigate the interaction between CAF and SB in water, a ^1H NMR titration experiment using CAF as host and SB as guest was performed in D_2O (Fig. 2, ESI Figure S2). The shift of all protons in CAF is significant while the overall shift of proton 1 and 2 is larger than that of proton 3 and 4 (ESI Table S3). Since protons 1, 2 and 3, 4 are in the five-membered (CAF5, ring B in Fig. 2a) and six-membered ring (CAF6, ring A in Fig. 2a) of CAF respectively, the result indicates the chemical environment of the CAF5 changes most with the addition of SB. Due to the lack of a strong hydrogen bond donor in both CAF and SB, it is unlikely that a hydrogen bond is formed between the two molecules. The large shift of CAF protons can be explained by the presence of π stackings and the larger shift observed on the five-membered ring may be a result of the greater change in the chemical environment of the ring caused by the π stackings.

To ensure that the observed significant peak shift is indeed due to CAF interacting with SB and not dilution of CAF, a control ^1H NMR titration was performed using the same concentrations but exchanging the guest from SB solution to a dilution with an equivalent volume of pure D_2O (ESI Table S4). The result shows negligible peak shift of CAF protons due to the dilution.

Multiple models with interactions of different stoichiometry, 1:1, 2:1 and 1:2 host:guest ratio, were used to fit the measured peak shifts (Table 1), with all three models resulting in a reasonable fit. The 1:1 model shows the least error but results in a very small apparent binding constant K_{11}, leading to a positive apparent Gibbs free binding energy $\Delta G_{bind.}$ This would indicate that the aggregation between CAF and SB is not favored, a result that does not match with the significant chemical shift of protons observed. However, 1:1 aggregates with a small K_{11} and positive ΔG_{bind} can further attract molecules of either species leading to aggregates with higher stoichiometry. If these are easier to form than the initial aggregate, i.e. the further apparent binding constant is larger than K_{11}, it should result in a more logical fit of the higher binding models (Martin, 1996). In the 1:2 model, the second apparent binding constant (K_{12}) is also small and with large error, showing that it is not the suitable model for the same reasons as for the pure 1:1 binding. The 2:1 model is

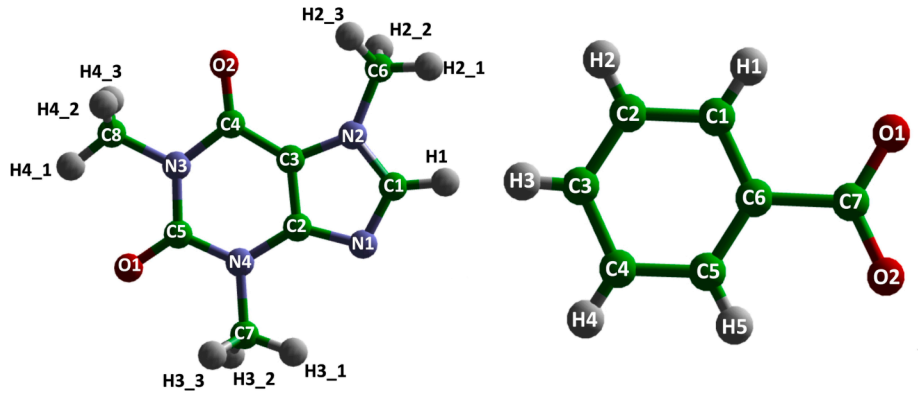

Fig. 1. CAF (left) and BEN (right) molecules labelled with atomic sites. (Carbon in green, nitrogen in blue, oxygen in red and hydrogen in grey). (For interpretation of the references to colour in this figure legend, the reader is referred to the web version of this article.)

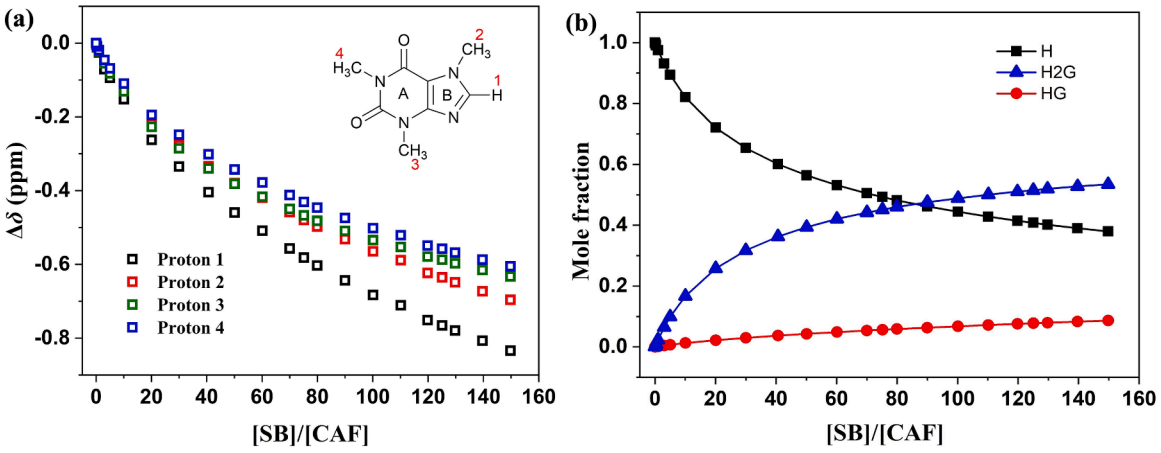

Fig. 2. (a) ^{1}H NMR peak shift of CAF protons 1–4 in CAF-SB titration in D_2O (Proton naming according to Scheme 1); (b) speciation plot of NMR titration data fitted by 2:1 binding model.

Table 1
Binding constants and calculated ΔG_{bind} of all protons in in D_2O using different binding models.

[H]:[G] binding model	K_{11} (M^{-1}) (±% error)	K_{12} (M^{-1}) (±% error)	K_{21} (M^{-1}) (±% error)	Δ G_{bind} (kJ/mol) (±% error)
1:1	0.57 (±1.0 %)	N/A	N/A	1.37 (±3.6 %)
1:2	2.79 (±2.3 %)	0.17 (±9.4 %)	N/A	−2.5 (±0.4 %)
2:1	0.73 (±2.5 %)	N/A	440 (±4.1 %)	−14.8 (±1.4 %)

the best fitting model with the K_{11} of 0.73 M^{-1}, similar to the value of the 1:1 model, and a large K_{21} of 440 M^{-1}. The calculated energy Δ G_{bind} = –14.8 kJ/mol shows strong interaction between CAF and SB in water, which is in agreement with the significant experimental shifts. The speciation plot of the 2:1 model shows a high overall aggregation between the two compounds (Fig. 2b), among which the 2:1 complex is with 50% dominant compared with the 1:1 complex and pure CAF. Moreover, it is obvious that the 2:1 complex form faster after initial formation of the 1:1 aggregate, resulting in an overall low concentration of the 1:1 aggregate in solution.

3.3. Neutron total scattering

To gain further insight into the exact stoichiometry and the structure of the aggregates forming in solution, we performed neutron total scattering on the solution samples at 25 °C. The used solution concentration was chosen in the higher SB concentrations (4 M), which lie in the second part of solubility enhancement and hence small variations due to experimental error should have a low impact on the hydrotropism. Furthermore, the limitation of neutron total scattering is that the observed species needs to represent at least 5 mol% of all hydrogen atoms of the sample to enable appropriate modelling. The chosen solution concentration satisfies this requirement. An empirical potential structure refinement simulation was fitted to the experimental data using Dissolve. The comparison of the calculated to the experimental interference differential cross section $F(Q)$ (Fig. 3a) shows a close fit with only minor discrepancies in the intensities of the peaks. The small differences in the low-Q region (<2.5 Å) are likely due to the subtraction of the inelastic and incoherent scattering of protium in the samples (Bowron and Moreno, 2002). It has been shown that these differences do not affect the overall structural model at the intermolecular length scales as the introduced systematic error in real space distance is negligibly small (Bowron and Moreno, 2002; Burton et al., 2009; Soper et al., 2003).

Furthermore, the fit on the pair distribution function $g(r)$ (Fig. 3b) obtained by Fourier transform of $F(Q)$ describes well the features of the experimental data, especially in the intramolecular distances indicating that the molecular model is sound.

A detailed interpretation of the solution structure of the ternary system can be based on the selected partial radial distribution functions (RDFs) $g_{\alpha\beta}(r)$, showing the spatial correlations between atoms α and β.

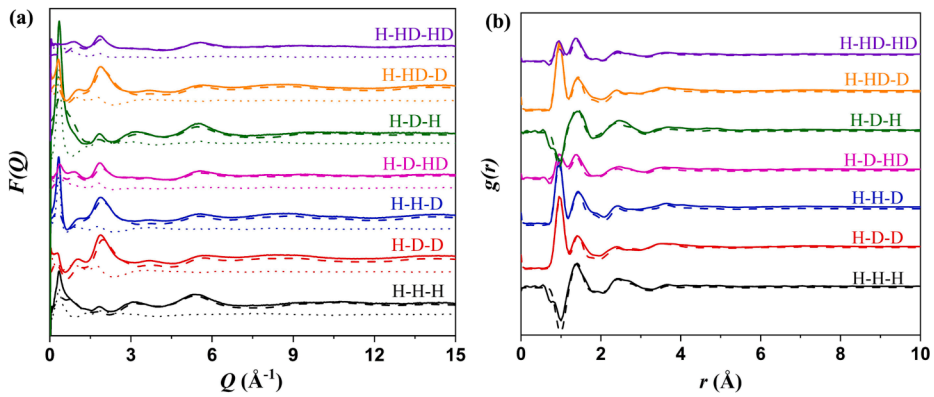

Fig. 3. (a) Experimentally measured $F(Q)$s (solid lines), Dissolve fits (dash lines), and residuals (dot lines) and (b) $g(r)$ determined by Fourier transform of experimental $F(Q)$ (solid lines) and Dissolve fits (dash lines) at 25 °C. Graphs are offset for clarity.

For clarity, intramolecular correlations are omitted. Of particular interest in our interpretation of the structural model are hydrogen bonds, π stacking and ionic interactions between the different solute species (CAF and SB) with each other and with the solvent, water. While simple RDFs between hydrogen bond donor, acceptor and ion give information about hydrogen bonds, for the ring-ring interactions the molecular center or a specific ring center is chosen to determine the distance distribution and the flat surfaces of the respective rings for the angle distribution.

3.3.1. *Solute-solute interaction*

The correlation between CAF molecules (Fig. 4a) shows that the distance of the two CAF planes is approximately 3.6–3.7 Å, which fits well with the distance of π stacking in the crystal structure (Zhao et al., 2015). This distance is not affected by the nature of the interaction involving the centre of either of the CAF two rings, CAF6 or CAF5. The correlation between the two central CAF carbons (C2, C3) (ESI Figure S3) shows a similar first peak as shown in pure caffeine (Tavagnacco et al., 2015). There is a comparable slight increase in intensity in

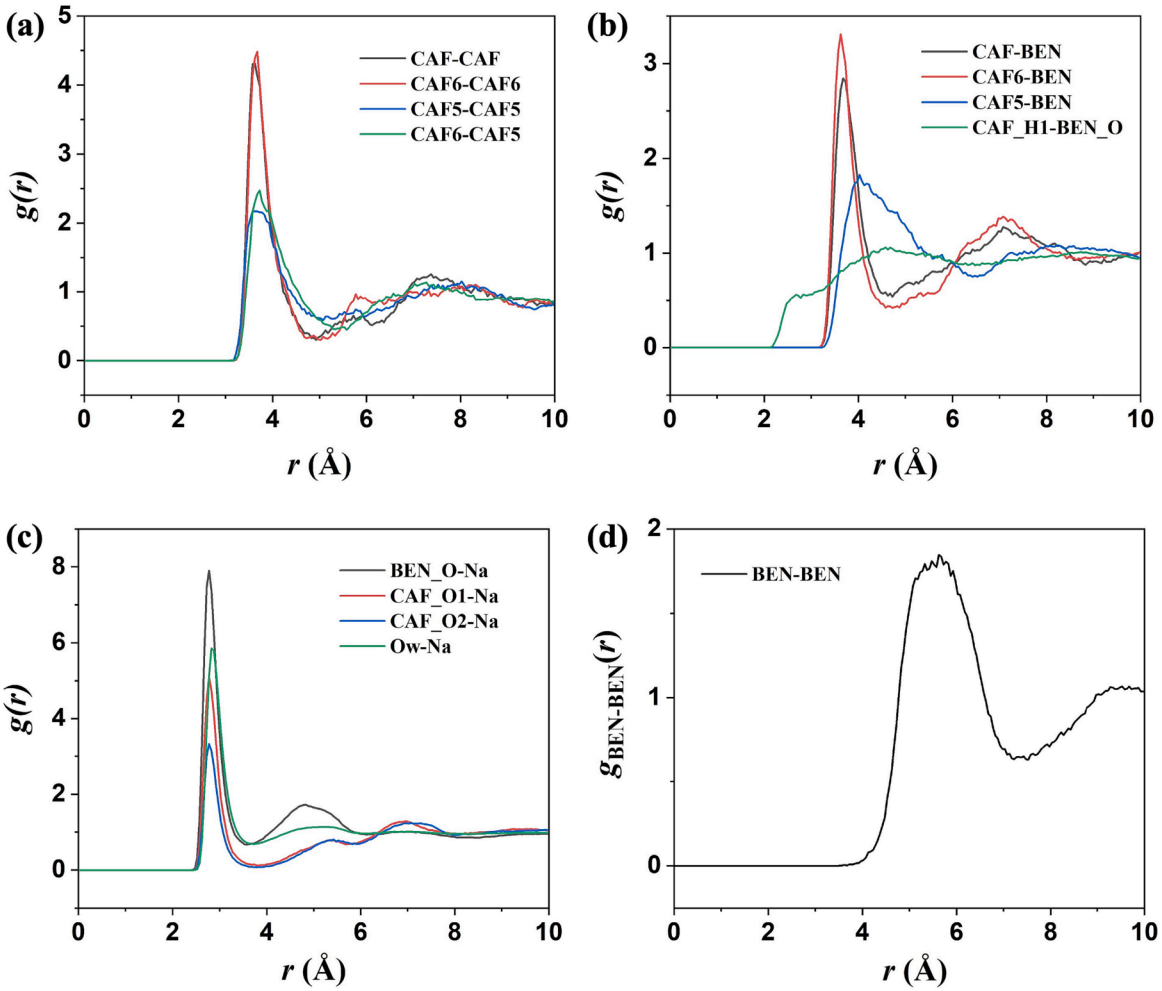

Fig. 4. Partial radial distribution functions of (a) CAF-CAF, (b) CAF-BEN, (c) O-Na^+ and (d) BEN-BEN for CAF and SB in water at 25 °C.

this close contact from C3-C3 to C2-C3 and then C2-C2, indicating that the zigzag configuration of CAF stacking in pure solution also exists in the presence of SB in our system. However, all these distances are shorter than have been previously found for pure caffeine in water at elevated temperature (Tavagnacco et al., 2015), which may be due either to the increased mobility of the molecules at these higher temperatures, or due to the presence of a second solute in our samples. The angle of the two interacting rings shows the highest population around 0° and 180 with a rather narrow distribution to 10° and 170° (ESI Figure S4), showing the two CAF rings are mainly parallel. Both the distance and angle prove the formation of π stacking among CAF molecules in solution. Using Dissolve, we can for the first time distinguish between the interactions around CAF5 and CAF6. Both ring RDFs show the peak position at the same distance, 3.68 and 3.66 Å, respectively. However, the lower-intensity and broader peak and lower co-ordination number in the CAF5-CAF5 interaction indicates significantly weaker stacking compared with CAF6-CAF6. The interaction between the two rings, CAF6-CAF5, shows comparably low distance to the CAF5-CAF5 interaction and a similar broadness indicating a less directional and less ordered interaction. The similar distance of CAF6-CAF5 stacking with CAF6-CAF6 and CAF5-CAF5 stacking indicates the π stacking is more likely to be off-set rather than face-to-face (ESI Figure S5), which is similar in the crystal structure of anhydrous caffeine (Lehmann and Stowasser, 2007). A further explanation would be anti-parallel stacking, which has been predicted to have lower energy than the parallel stacking (Carlucci and Gavezzotti, 2005) but never found experimentally. Finally, the coordination number of CAF self-stacking of approximately 0.4 indicates that there may be other interactions competing with the self-aggregation of CAF.

The second solute–solute interaction of interest is between CAF and BEN. The correlation between the centres of both molecules shows a sharp peak at 3.68 Å (Fig. 4b) with the angle peaking again at 0° and 180° (ESI Fig. S6a-c), clearly indicating π stacking between CAF and BEN rings. The presence of this interaction is consistent with the significant shift of CAF protons observed in the NMR titration experiment. The coordination number of approximately 0.5 corroborates the NMR fitting results that the 2:1 host:guest is the best model, indicating that a CAF-BEN 2:1 complex is likely to form in the solution. Due to the similar distance of the first peak between CAF-CAF and CAF-BEN stacking, the 2:1 complex is more likely to be a CAF-CAF-SB stacking (ESI Figure S7a), rather than a sandwich structure. Again, the model allows us to distinguish between the two rings in caffeine. The peak of CAF6-BEN is sharper and at shorter distance compared to CAF5-BEN, showing the interaction between CAF6 and BEN is stronger (ESI Figure S7b). In addition, the broadened CAF5-BEN peak indicates multiple interactions, which range from parallel stacking directly over the CAF5 ring to the charge-assisted hydrogen bond between the ring proton with the BEN, and also include the correlation with the BEN stacked on CAF6 at longer distance. Hence, the coordination number is significantly larger than for CAF6-BEN. Connecting this result with the proton shift observed in the NMR titration, in which protons on CAF5 have a larger chemical shift compared with those on CAF6, indicating that there is likely another interaction with CAF6 such as with Na^+ causing an opposite shift to that induced by BEN and leading to an apparent smaller shift on CAF6 protons. This hypothesis is corroborated by the RDFs of Na^+ (Fig. 4c). The cation can interact with both CAF and BEN solutes as well as with water through their respective oxygen atoms. The RDFs of all four correlations show sharp peaks at a similar distance between 2.77 and 2.82 Å. It is noticeable that the coordination number of sodium around the benzoate anion is only approximately 0.5 meaning that only half of benzoate anions are coordinating to the cation. This illustrates that even though in the solid, Na^+ combines with benzoate forming sodium benzoate salt, in the solution Na^+ is more likely to interact with either the oxygen atoms of CAF or water. Both carbonyl oxygen atoms of CAF show a similar $g(r)$ and coordination number with Na^+, therefore having almost equal probability to interact with Na^+. From these results, it is likely that both the stacking with the anionic BEN and Coulombic interaction with Na^+ are likely to lead the solubility enhancement of CAF due to an increased charged character of the stacking compared to pure CAF.

Another possible interaction to consider is a charge-assisted hydrogen bond between $H1_{(CAF)}$ and $O_{(BEN)}$. The proton H1 is the most acidic proton in CAF, and even though it is not a strong hydrogen-bond donor, it can be involved in solution interactions with benzoic acid (Shen et al., 2023). However, the RDF shows neither a significant peak (Fig. 4b) for a hydrogen bond nor the corresponding angles (ESI Figure S8a), hence this interaction is not favoured in solution. Comparably, the BEN anions are not significantly interacting in solution, as the first correlation peak in the BEN centre-of-ring RDF is broad and occurs at considerably longer distances than would be expected for π-stacking (Fig. 4d, ESI Fig. S6d). This is likely due to the repulsive force between the two BEN anions due to the charged carboxylates. It is clear that the proposed interaction of other hydrotrope molecules (Balasubramanian et al., 1989; Cui, 2010; Cui et al., 2010) is not the mechanism of solubility enhancement in this system.

3.3.2. Solute hydration shell

Another potential mechanism of hydrotropism is that the presence of SB alters the solvation shell around CAF and potentially increases the interaction of CAF with water. The $g_{CAF\_O1\text{-}Hw}(r)$ and $g_{CAF\_O2\text{-}Hw}(r)$ show the distances between CAF carbonyl oxygen atoms O1 and O2 to the water hydrogen atoms Hw (Table 2, Fig. 5 and ESI Figure S8). These functions show a first sharp peak at 1.77 Å with the corresponding angle centring around 180° (ESI Figure S8b-c), indicating a strong and linear interaction at the distance of standard to strong hydrogen bonds (Herschlag and Pinney, 2018). Furthermore, both interactions show a coordination number above 1, so the caffeine molecules are clearly hydrated. It is worth noting that the distances of these hydrogen bonds are significantly shorter than those of pure CAF in water, where they have been described to be around 2.05 Å (Tavagnacco et al., 2015). It is

Table 2
Peak position and average co-ordination number calculated from integration of partial distribution functions for CAF and SB in water at 25 °C. Hw and Ow are H and O atoms of water, respectively.

Correlation	r_{peak} (Å)	r_{min}(Å)	r_{max} (Å)	Co-ordination number (atoms)
CAF-CAF	3.6	3	5	0.39 ± 0.05
CAF6-CAF6	3.68	3	5	0.39 ± 0.06
CAF5-CAF5	3.66	3	4.5	0.27 ± 0.03
CAF6-CAF5	3.73	3	5.7	0.47 ± 0.05
C2-C2	3.78	3	6	0.80 ± 0.14
C2-C3	3.72	3	6	0.78 ± 0.10
C3-C3	3.67	3	6	0.76 ± 0.09
CAF-BEN	3.68	3	4.5	0.49 ± 0.04
CAF6-BEN	3.62	3	5	0.58 ± 0.04
CAF5-BEN	4.03	3	6.5	1.57 ± 0.07
CAF_H1-BEN_O	N/A	2	3	0.09 ± 0.03
BEN_O-Na	2.77	2	3.6	0.49 ± 0.03
CAF_O1-Na	2.78	2	3.8	0.29 ± 0.03
CAF_O2-Na	2.77	2	4	0.20 ± 0.02
Ow-Na	2.82	2	3.7	0.43 ± 0.00
BEN-BEN	5.53	3	7.5	2.31 ± 0.07
CAF_O1-Hw	1.77	1	2.5	1.29 ± 0.05
CAF_O2-Hw	1.78	1	2.5	1.23 ± 0.05
CAF_N1-Hw	1.97	1	2.6	0.79 ± 0.06
CAF_H1-Ow	2.79	2	4.4	5.03 ± 0.18 [a]
BEN_O-Hw	1.72	1	2.4	2.63 ± 0.03
Na-Hw	3.46	2	4.5	16.6 ± 2.1 [a]
Na-Ow	2.83	2	3.7	4.76 ± 1.41
Hw-Hw	2.47	1	3	4.34 ± 0.02 [a]
Hw-Ow	1.82	1	2.4	0.68 ± 0.00
Ow-Ow	2.77	2	3.2	3.11 ± 0.02

[a] the large coordination numbers of CAF_H1-Ow, Na-Hw and Hw-Hw do not represent a single interaction but the random location of water oxygen and hydrogen atoms around CAF_H1 and Na^+ due to the broadness of the peak in the RDF.

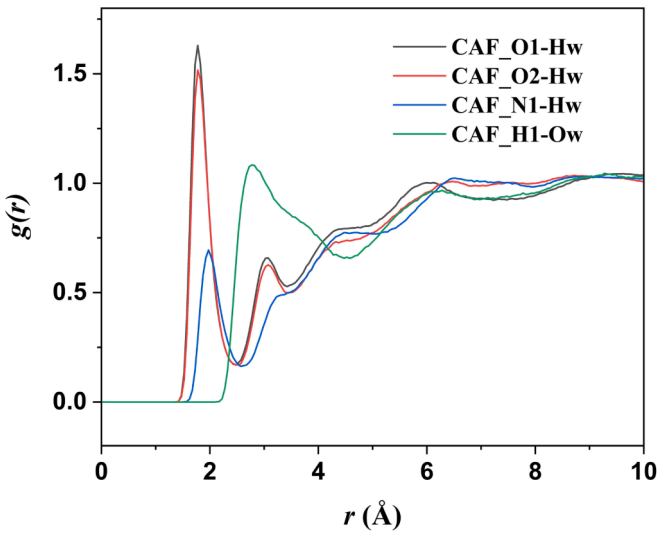

Fig. 5. Partial radial distribution functions of CAF-water for CAF and SB in water at 25 °C.

thus clear that the presence of SB increases the strength of the CAF-water interaction, potentially through enabling charge-assisted hydrogen bonds, e.g. through water molecules bridging between the charged BEN and the uncharged CAF molecules (ESI Figure S9).

Further to the carbonyl moieties, CAF can accept hydrogen bonds from water to the ring nitrogen atom N1. This interaction can be found in the CAF hydrate crystal structure (Edwards et al., 1997), indicating that it is a strong interaction that potentially can be found in solution as well. From the simulation, $g_{N1\text{-}Hw}(r)$ shows the first peak at 1.97 Å with the angle plot again indicating the linearity of this interaction (Fig. 5, ESI Figure S8d). However, this hydrogen bond is significantly longer than those involving O1 and O2 and is thus unlikely to be a dominant influence in increasing the solubility.

The CAF_H1 and water interaction is the weakest with the longer distance of almost 2 Å, a much broader first peak and a lack of directionality (Fig. 5, ESI Figure S8e). From this data, it is unlikely that a hydrogen bond is formed involving the acidic proton of CAF. It is possible that the stronger peak shift observed by ^{1}H NMR titration is due to a change in the hydration around this proton, but further studies are necessary to prove this hypothesis.

The water coordination around the strong hydrogen bond acceptor BEN shows an intense and sharp peak at 1.72 Å with a narrow peak at 180° (Fig. 6a and ESI Figure S8f). This indicates the anticipated strong hydrogen-bond interaction. The coordination number of 2.6 shows that BEN is clearly hydrated. The strong hydrogen bond between BEN and water will polarize the water in the direct vicinity of BEN, and since we have shown above that BEN and CAF will form π-stacks, it is likely that this polarization will strengthen the CAF-water hydrogen bonds in turn (ESI Figure S10).

It is well-known that sodium cations will coordinate to water, and we can see the same behaviour in the $g_{Na\text{-}Ow}(r)$ and $g_{Na\text{-}Hw}(r)$. The first coordination shell shows a very strong and narrow peak with a Na^+-Ow distance of 2.83 Å. The distance to the water hydrogen atoms Hw is slightly longer at 3.46 Å clearly indicating that the coordination to the water oxygen Ow is realized. Surprisingly, both of these distances are longer than those reported previously for NaOH/water system (Botti et al., 2004; McLain et al., 2006). Moreover, the coordination number of $g_{Na\text{-}Ow}(r)$ is 4.76 ± 1.41, smaller than that of the Na^+-water interaction in absence of strongly interacting anions, which is 5.5 ± 0.5 (Wang et al., 2019). The shift of the first hydration shell of Na^+ to longer distance and the lower coordination number indicate weaker Coulombic interaction between the cation and water, which could be explained by a longer-lived coordination to the BEN anion and hence partial charge-shielding (ESI Figure S11).

3.3.3. *Water structure*

It has been shown that the addition of charged solutes can change the overall structure of water due to chemical pressure (Laurent et al., 2021; Lenton et al., 2017). The change of the water structure could also be a factor in hydrotropism (Cui, 2010; Dhapte and Mehta, 2015). The partial radial distribution functions for water-water interactions in our samples were simulated (Fig. 6b) and the peak position and coordination number were compared with those of pure water (Soper and Phillips, 1986) and

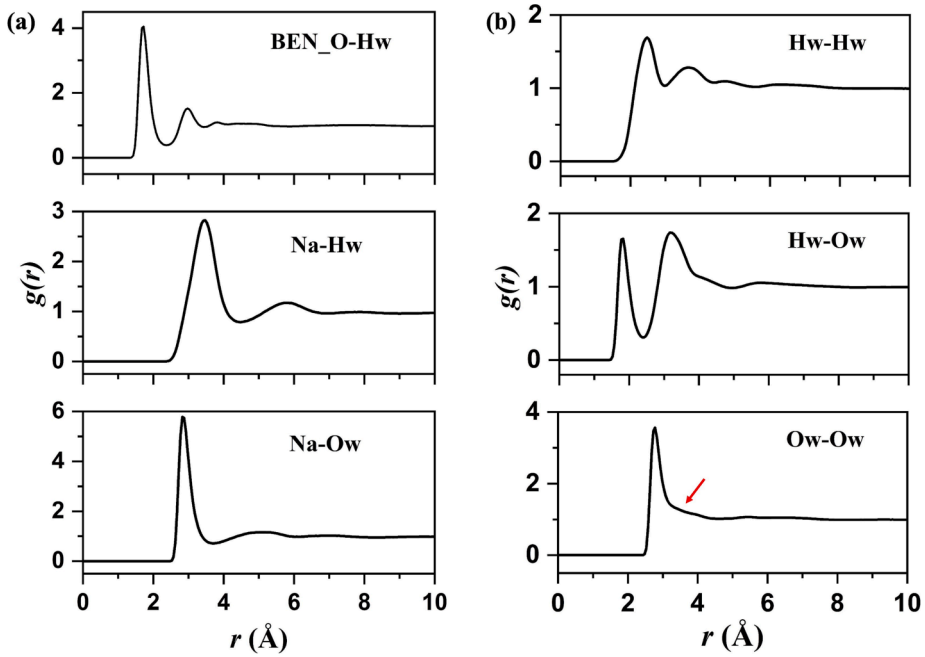

Fig. 6. Partial radial distribution functions of (a) solute-water interactions: Top – BEN-water, middle – Na-Hw and bottom – Na-Ow; and (b) water-water interactions: Top – Hw-Hw, middle – Hw-Ow and bottom – Ow-Ow at 25 °C.

2 M NaOH aqueous solution (McLain et al., 2006) (Table 3). Surprisingly, both $g_{Ow\text{-}Hw}(r)$ and $g_{Ow\text{-}Ow}(r)$ show differences, most pronounced in the latter. While the distance of the first solvation shell in $g_{Ow\text{-}Hw}(r)$ is comparable to that in pure water, the coordination number of this shell is reduced. This is likely due to the competition in hydrogen bonding in the presence of additional solute molecules, in our case both CAF and BEN. For $g_{Ow\text{-}Ow}(r)$ the first interaction peak distance and the coordination number of this interaction are significantly reduced compared to pure water. The presence of charged species cannot be taken as explanation here, as the sample of 2 M NaOH in water shows a longer distance for this closest interaction. It is possible that the presence of charge-assisted hydrogen bond interaction between BEN and water leads to a reduction of the hydrogen-bonding distance between water molecules and hence a lower distance between water molecules (ESI Figure S12). This interpretation is corroborated by the reduced coordination number in the $g_{Ow\text{-}Hw}(r)$ indicating a reduced hydrogen bonding. The difference of $g_{Hw\text{-}Hw}(r)$ in our system and pure water is not significant but shows a significantly shorter distance in the first hydration shell compared to 2 M NaOH. In the first solvation shell, the water structure in CAF-SB is closer related to that of pure water than that in aqueous NaOH at a comparable concentration.

A particular difference found in samples of water under chemical pressure is the tightening of the second solvation shell as indicated by the shift of the second interaction peak in the $g(r)$ to shorter distances (Laurent et al., 2022; Lenton et al., 2017). The same behaviour can be observed in our samples (Fig. 6b arrow), and the shape of the relevant peak is similar to that of higher concentration of NaOH in water (Botti et al., 2004). The peak at 4.3 Å in the $g_{Ow\text{-}Ow}(r)$ in pure water at ambient conditions corresponds to an extended tetrahedral hydrogen bond network and this interaction and hydration shell can be distorted and broken by external high pressure (Soper and Ricci, 2000). The effect of the charged species in highly concentrated ionic solutions on the water structure is similar to that of the external high pressure (Botti et al., 2004). In our solution, both CAF and SB are present in high concentration and can form strong hydrogen bonds with water. Therefore, the water molecules engage in the hydration shell of CAF, BEN and Na^+, which is consistent with the result of solute–solvent interaction mentioned above, and there are fewer water molecules available to form the second or further hydration shell around water. The changes in water structure show again the strong hydrogen bond interaction between the CAF-BEN aggregates as well as the individual solute molecules/ions and water improving the solubility of CAF in water.

4. Conclusion

The solubility of caffeine at room temperature can be enhanced more than 20 folds by the addition of sodium benzoate acting as a hydrotrope. We found that the ^{1}H NMR titration using CAF as host and SB as guest in D_2O shows significant shift of all CAF protons and large apparent binding constant and apparent Gibbs free binding energy of –14.8 kJ/mol after fitting, indicating strong heteromeric interaction within a 2:1 CAF-SB complex. The result is corroborated by the neutron total scattering data of CAF-BEN. The correlation $g_{CAF\text{-}BEN}(r)$ clearly shows the π stacking between CAF and BEN rings with the coordination number 0.49 ± 0.04 which translates into a 2:1 stacking. The six-membered ring (CAF6) interacts stronger with BEN compared the five-membered ring (CAF5) as indicated by sharper and shorter RDF peak. In addition, Na^+ shows Coulombic interaction with both carboxylic oxygen atoms of CAF in solution. The RDF of BEN-water shows the shortest peak and strongest hydrogen bond interaction among all interactions in solution, helping to stabilise the CAF-SB complex in solution and therefore raising the solubility of CAF in water. Moreover, the shorter hydrogen bond distance between CAF and water compared with that in pure CAF solution (Tavagnacco et al., 2015) is likely to be supported by the polarization of water molecules hydrogen-bonding to BEN, and supports the increased solubility of CAF. The collapse of the second hydration shell of water is observed in water-water correlations due to the presence of CAF and SB, again showing their strong interaction with water comparable to the chemical pressure exerted by highly concentrated ionic solutions. Overall, the hydrotropism behaviour of CAF-SB system has been unveiled as being a combination of hydrotrope stacking with the solute, increased hydration of the solute due to the hydrotrope, and a change in water structure. It is not clear, however, which of these mechanisms is the dominant. It has to be mentioned that there are many pharmaceutically relevant compounds with lower solubility than CAF making them more relevant for hydrotropism. Unfortunately, the limitation of neutron total scattering experiments is in the low interaction of neutron radiation with matter and hence the studied solutions need to contain at least 5 mol% hydrogen from the species that should be modelled to get the reliable structural data. This requirement is fulfilled for both CAF and SB making these solutions good model systems. By using NMR spectroscopy in combination with neutron total scattering, we could uncover both energetic and structural aspects of the solution aggregation of CAF-SB in water. Both are promising and complementary techniques to further explore hydrotropism phenomena of compounds with lower solubility, for which hydrotropism is pharmaceutically more relevant.

Table 3
First peak distance and coordination number (CN) for water radial distribution functions for water system, NaOH/water system and CAF/SB/water system.

RDF	CAF-SB + water		Water (Soper and Phillips, 1986)		NaOH + Water (McLain et al., 2006)	
	r_{peak} (Å)	CN	r_{peak} (Å)	CN	r_{peak} (Å)	CN
$g_{Hw\text{-}Hw}(r)$	2.47	4.34	2.45	4–5	2.85	4.1
$g_{Ow\text{-}Hw}(r)$	1.82	1.47	1.85	1.8	2.37	1.6
$g_{Ow\text{-}Ow}(r)$	2.77	3.11	2.975	4.5	3.36	4.2

CRediT authorship contribution statement

Yichun Shen: Writing – original draft, Investigation, Methodology, Validation, Formal analysis. **Yitian Xiao:** Investigation, Formal analysis, Validation. **Robert M. Edkins:** Writing – review & editing, Resources. **Tristan G.A. Youngs:** Writing – review & editing, Resources, Formal analysis. **Terri-Louise Hughes:** Writing – review & editing, Resources. **James Tellam:** Writing – review & editing, Resources. **Katharina Edkins:** Conceptualization, Writing – review & editing, Resources, Supervision.

Declaration of Competing Interest

The authors declare that they have no known competing financial interests or personal relationships that could have appeared to influence the work reported in this paper.

Data availability

Data is available at DOI.org/10.5286/ISIS.E.RB2220107

Acknowledgement

Y.S thanks the China Scholarship Council (CSC) (202006250018) for funding. We thank STFC for access to neutron beamtime on NIMROD at the ISIS Neutron and Muon Facility through the proposal RB2220107 (https://doi.org/10.5286/ISIS.E.RB2220107).

Appendix A. Supplementary data

Supplementary data to this article can be found online at https://doi.org/10.1016/j.ijpharm.2023.123520.

References

Aakeroy, C.B., Forbes, S., Desper, J., 2009. Using Cocrystals To Systematically Modulate Aqueous Solubility and Melting Behavior of an Anticancer Drug. J. Am. Chem. Soc. 131, 17048–17049.

Alshora, D.H., Ibrahim, M.A., Alanazi, F.K., 2016. Chapter 6 - Nanotechnology from particle size reduction to enhancing aqueous solubility. In: Grumezescu, A.M. (Ed.), Surface Chemistry of Nanobiomaterials. William Andrew Publishing, pp. 163–191.

Balasubramanian, D., Srinivas, V., Gaikar, V.G., Sharma, M.M., 1989. Aggregation behavior of hydrotropic compounds in aqueous solution. J. Phys. Chem. 93, 3865–3870.

Botti, A., Bruni, F., Imberti, S., Ricci, M.A., Soper, A.K., 2004. Ions in water: The microscopic structure of concentrated NaOH solutions. J. Chem. Phys. 120, 10154–10162.

Bowron, D.T., Moreno, S.D.a., 2002. The structure of a concentrated aqueous solution of tertiary butanol: Water pockets and resulting perturbations. J. Chem. Phys. 117, 3753–3762.

Brocos, P., Díaz-Vergara, N., Banquy, X., Pérez-Casas, S., Costas, M., Piñeiro, Á., 2010. Similarities and differences between cyclodextrin−sodium dodecyl sulfate host−guest complexes of different stoichiometries: molecular dynamics simulations at several temperatures. J. Phys. Chem. B 114, 12455–12467.

Burton, R.C., Ferrari, E.S., Davey, R.J., Finney, J.L., Bowron, D.T., 2009. Relationship between solution structure and phase behavior: A neutron scattering study of concentrated aqueous hexamethylenetetramine solutions. J. Phys. Chem. B 113, 5967–5977.

Carlucci, L., Gavezzotti, A., 2005. Molecular recognition and crystal energy landscapes: An X-ray and computational study of caffeine and other methylxanthines. Chem Eur J 11, 271–279.

Cheng, T.K., Coon, C.N., 1990. Effect of calcium source, particle size, limestone solubility in vitro, and calcium intake level on layer bone status and performance1. Poult. Sci. 69, 2214–2219.

Coffman, R.E., Kildsig, D.O., 1996. Hydrotropic solubilization— mechanistic studies. Pharm. Res. 13, 1460–1463.

Cui, Y., 2010. Parallel stacking of caffeine with riboflavin in aqueous solutions: The potential mechanism for hydrotropic solubilization of riboflavin. Int. J. Pharm. 397, 36–43.

Cui, Y., Xing, C., Ran, Y., 2010. Molecular dynamics simulations of hydrotropic solubilization and self-aggregation of nicotinamide. J. Pharm. Sci. 99, 3048–3059.

Dhapte, V., Mehta, P., 2015. Advances in hydrotropic solutions: An updated review. St. Petersburg Polytechnical University Journal: Physics and Mathematics 1, 424–435.

Edwards, H.G.M., Lawson, E., deMatas, M., Shields, L., York, P., 1997. Metamorphosis of caffeine hydrate and anhydrous caffeine. J. Chem. Soc Perkin trans 1985–1990.

Gorodischer, R., Karplus, M., 1982. Pharmacokinetic aspects of caffeine in premature infants with apnoea. Eur. J. Clin. Pharmacol. 22, 47–52.

Guerrero-Martínez, A., González-Gaitano, G., Viñas, M.H., Tardajos, G., 2006. Inclusion complexes between β-cyclodextrin and a gemini surfactant in aqueous solution: An NMR study. J. Phys. Chem. B 110, 13819–13828.

Han, Y., Pan, N., Li, D., Liu, S., Sun, B., Chai, J., Li, D., 2022. Formation mechanism of surfactant-free microemulsion and a judgment on whether it can be formed in one ternary system. J. Chem. Eng. 437, 135385.

Herschlag, D., Pinney, M.M., 2018. Hydrogen bonds: Simple after All? Biochemistry 57, 3338–3352.

Hodgdon, T.K., Kaler, E.W., 2007. Hydrotropic solutions. Curr. Opin. Colloid Interface Sci. 12, 121–128.

Hopkins Hatzopoulos, M., Eastoe, J., Dowding, P.J., Rogers, S.E., Heenan, R., Dyer, R., 2011. Are hydrotropes distinct from surfactants? Langmuir 27, 12346–12353.

Hussain, M.A., Diluccio, R.C., Maurin, M.B., 1993. Complexation of moricizine with nicotinamide and evaluation of the complexation constants by various methods. J. Pharm. Sci. 82, 77–79.

Jangid, A.K., Agraval, H., Gupta, N., Yadav, U.C.S., Sistla, R., Pooja, D., Kulhari, H., 2019. Designing of fatty acid-surfactant conjugate based nanomicelles of morin hydrate for simultaneously enhancing anticancer activity and oral bioavailability. Colloids Surf. B Biointerfaces 175, 202–211.

Könczöl, Á., Dargó, G., 2018. Brief overview of solubility methods: Recent trends in equilibrium solubility measurement and predictive models. Drug Discov. Today Technol. 27, 3–10.

Kumar, D., Khan, F., Rub, M.A., Azum, N., Asiri, A.M., 2021. Interactions between promethazine hydrochloride drug and sodium benzoate hydrotrope mixtures in various solvent media at different temperatures. J. Mol. Liq. 325, 115188.

Kunz, W., Holmberg, K., Zemb, T., 2016. Hydrotropes. Curr. Opin. Colloid Interface Sci. 22, 99–107.

Laurent, H., Baker, D.L., Soper, A.K., Ries, M.E., Dougan, L., 2021. Bridging structure, dynamics, and thermodynamics: An example study on aqueous potassium halides. J. Phys. Chem. B 125, 12774–12786.

Laurent, H., Youngs, T.G.A., Headen, T.F., Soper, A.K., Dougan, L., 2022. The ability of trimethylamine N-oxide to resist pressure induced perturbations to water structure. Commun. Chem. 5, 116.

Lee, J.W., Lee, S.C., Acharya, G., Chang, C.J., Park, K., 2003. Hydrotropic solubilization of paclitaxel: Analysis of chemical structures for hydrotropic property. Pharm. Res. 20, 1022–1030.

Lehmann, C.W., Stowasser, F., 2007. The Crystal Structure of Anhydrous β-Caffeine as Determined from X-ray Powder-Diffraction Data. Chem Eur J 13, 2908–2911.

Lenton, S., Rhys, N.H., Towey, J.J., Soper, A.K., Dougan, L., 2017. Highly compressed water structure observed in a perchlorate aqueous solution. Nat. Commun. 8, 919.

Loh, Z.H., Samanta, A.K., Heng, P.W.S., 2015. Overview of milling techniques for improving the solubility of poorly water-soluble drugs. Asian J. Pharm. Sci. 10, 255–274.

Lu, Y.P., Lou, Y.R., Xie, J.G., Peng, Q.Y., Zhou, S., Lin, Y., Shih, W.J., Conney, A.H., 2007. Caffeine and caffeine sodium benzoate have a sunscreen effect, enhance UVB-induced apoptosis, and inhibit UVB-induced skin carcinogenesis in SKH-1 mice. Carcinogenesis 28, 199–206.

Martin, R.B., 1996. Comparisons of Indefinite Self-Association Models. Chem. Rev. 96, 3043–3064.

Martinez, L.M., Cruz-Angeles, J., Vazquez-Davila, M., Martinez, E., Cabada, P., Navarrete-Bernal, C., Cortez, F., 2022. Mechanical activation by ball milling as a strategy to prepare highly soluble pharmaceutical formulations in the form of co-amorphous, co-crystals, or polymorphs. Pharmaceutics 14.

McLain, S.E., Imberti, S., Soper, A.K., Botti, A., Bruni, F., Ricci, M.A., 2006. Structure of 2 molar NaOH in aqueous solution from neutron diffraction and empirical potential structure refinement. Phys. Rev. B 74.

Mishra, D.K., Dhote, V., Bhargava, A., Jain, D.K., Mishra, P.K., 2015. Amorphous solid dispersion technique for improved drug delivery: basics to clinical applications. Drug Deliv. Transl. Res. 5, 552–565.

Misra, S.K., Pathak, K., 2020. Supercritical fluid technology for solubilization of poorly water soluble drugs via micro- and naonosized particle generation. Admet and Dmpk 8, 355–374.

Park, S.I., Lee, K.W., Park, S., Shin, M.S., Park, B.S., 2022. Aqueous solubility of high concentrated caffeine using hydrotrope and the application to the anti-cellulite cosmetics. Int. J. Advances Appl. Sci. 9, 79–85.

Rasool, A.A., Hussain, A.A., Dittert, L.W., 1991. Solubility Enhancement of Some Water-Insoluble Drugs in the Presence of Nicotinamide and Related Compounds. J. Pharm. Sci. 80, 387–393.

Rub, M.A., 2020. Effect of additives on the aggregation phenomena of amphiphilic drug and hydrotrope mixtures. J. Mol. Liq. 298, 112049.

Sanghvi, R., Evans, D., Yalkowsky, S.H., 2007. Stacking complexation by nicotinamide: A useful way of enhancing drug solubility. Int. J. Pharm. 336, 35–41.

Savjani, K.T., Gajjar, A.K., Savjani, J.K., 2012. Drug solubility: Importance and enhancement techniques. ISRN Pharmaceutics 2012, 195727.

Serajuddin, A.T.M., 2007. Salt formation to improve drug solubility. Adv. Drug Deliv. Rev. 59, 603–616.

Shen, Y., Cruz-Cabeza, A.J., Azzouz, O., Edkins, K., 2023. Using prenucleation aggregation of caffeine-benzoic acid as a rapid indication of Co-crystallization from solutions. Mol. Pharm. 20, 1942–1950.

Shimizu, S., Matubayasi, N., 2014. Hydrotropy: Monomer-micelle equilibrium and minimum hydrotrope concentration. J. Phys. Chem. B 118, 10515–10524.

Shimizu, S., Matubayasi, N., 2017. Hydrotropy and scattering: pre-ouzo as an extended near-spinodal region. PCCP 19, 26734–26742.

Soper, A.K., 1996. Empirical potential Monte Carlo simulation of fluid structure. Chem. Phys. 202, 295–306.

Soper, A.K., Ricci, M.A., 2000. Structures of high-density and low-density water. Phys. Rev. Lett. 84, 2881–2884.

Soper, A.K., Castner, E.W., Luzar, A., 2003. Impact of urea on water structure: a clue to its properties as a denaturant? Biophys. Chem. 105, 649–666.

Soper, A.K., Phillips, M.G., 1986. A new determination of the structure of water at 25°C. Chem. Phys. 107, 47–60.

Subbarao, C.V., Chakravarthy, I.P.K., Bharadwaj, A., Prasad, K., 2012. Functions of hydrotropes in solutions. Chem. Eng. Technol. 35, 225–237.

Tavagnacco, L., Brady, J.W., Bruni, F., Callear, S., Ricci, M.A., Saboungi, M.L., Cesàro, A., 2015. Hydration of caffeine at high temperature by neutron scattering and simulation studies. J. Phys. Chem. B 119, 13294–13301.

Telange, D.R., Patil, A.T., Pethe, A.M., Fegade, H., Anand, S., Dave, V.S., 2017. Formulation and characterization of an apigenin-phospholipid phytosome (APLC) for improved solubility, in vivo bioavailability, and antioxidant potential. Eur. J. Pharm. Sci. 108, 36–49.

Thakuria, R., Delori, A., Jones, W., Lipert, M.P., Roy, L., Rodriguez-Hornedo, N., 2013. Pharmaceutical cocrystals and poorly soluble drugs. Int. J. Pharm. 453, 101–125.

Thordarson, P., 2011. Determining association constants from titration experiments in supramolecular chemistry (vol 40, pg 1305, 2011). Chem. Soc. Rev. 40, 5922–5923.

Tripathi, D., Sharma, D.K., Sahoo, J., Raman, S.K., 2022. Enhanced solubility of meloxicam with sodium benzoate hydrotrope: Ecofriendly approach for improved topical drug delivery. Indian J. Pharm. Educ. Res. 56, 1052–1062.

Varun Raj Vemula, V.L., Lingala, Srikanth, 2010. Solubility enhancement techniques. Int. J. Pharm. Sci. Rev. Res. 5, 41–51.

Wang, P., Shi, R., Su, Y., Tang, L., Huang, X., Zhao, J., 2019. Hydrated sodium ion clusters [Na+(H2O)n (n = 1–6)]: An ab initio study on structures and non-covalent interaction. Front Chem 7.

Yamamoto, K., Kojima, T., Karashima, M., Ikeda, Y., 2016. Physicochemical evaluation and developability assessment of Co-amorphouses of low soluble drugs and comparison to the Co-crystals. Chem. Pharm. Bull. 64, 1739–1746.

Youngs, T.G.A., 2010. Aten—An application for the creation, editing, and visualization of coordinates for glasses, liquids, crystals, and molecules. J. Comput. Chem. 31, 639–648.

Youngs, T., 2019. Dissolve: next generation software for the interrogation of total scattering data by empirical potential generation. Mol. Phys. 117, 3464–3477.

Yucel, A., Ozyalcin, S., Talu, G.K., Yucel, E.C., Erdine, S., 1999. Intravenous administration of caffeine sodium benzoate for postdural puncture headache. Reg. Anesth. Pain Med. 24, 51–54.
Zemb, T.N., Klossek, M., Lopian, T., Marcus, J., Schöettl, S., Horinek, D., Prevost, S.F., Touraud, D., Diat, O., Marčelja, S., Kunz, W., 2016. How to explain microemulsions formed by solvent mixtures without conventional surfactants. Proc. Natl. Acad. Sci. 113, 4260–4265.
Zhao, Y., Li, J., Gu, H., Wei, D., Xu, Y.-C., Fu, W., Yu, Z., 2015. Conformational preferences of π–π stacking between ligand and protein, analysis derived from crystal structure data geometric preference of π–π interaction. Interdiscip. Sci. Comput. Life Sci. 7, 211–220.